Pseudogap in cuprates driven by d-wave flux-phase order proximity effects: A theoretical analysis from Raman and ARPES experiments

Andrés Greco and Matías Bejas

Facultad de Ciencias Exactas, Ingeniería y Agrimensura and Instituto de Física Rosario (UNR-CONICET), Avenida Pellegrini 250, 2000 Rosario, Argentina

E-mail: `agreco@fceia.unr.edu.ar` and `bejas@ifir-conicet.gov.ar`

Abstract. One of the puzzling characteristics of the pseudogap phase of high-T_c cuprates is the nodal-antinodal dichotomy. While the nodal quasiparticles have a Fermi liquid behaviour, the antinodal ones show non-Fermi liquid features and an associated pseudogap. Angle-resolved photoemission spectroscopy and electronic Raman scattering are two valuable tools which have shown universal features which are rather material-independent, and presumably intrinsic to the pseudogap phase. The doping and temperature dependence of the Fermi arcs and the pseudogap observed by photoemission near the antinode correlates with the non-Fermi liquid behaviour observed by Raman for the B_{1g} mode. In contrast, and similar to the nodal quasiparticles detected by photoemission, the Raman B_{2g} mode shows Fermi liquid features. We show that these two experiments can be analysed, in the context of the t-J model, by self-energy effects in the proximity to a d-wave flux-phase order instability. This approach supports a crossover origin for the pseudogap, and a scenario of two competing phases. The B_{2g} mode shows, in an underdoped case, a depletion at intermediate energy which has attracted a renewed interest. We study this depletion and discuss its origin and relation with the pseudogap.

1. Introduction

Most of the experimental probes in the normal state of underdoped (UD) cuprates show signatures of a pseudogap (PG), a gap-like feature that appears below a characteristic temperature known generically as the pseudogap temperature T^*. Below this temperature the electronic properties are very unusual [1]. The value of T^* may depend on the experimental probe, and it is far above the superconducting critical temperature T_c. In contrast to the behaviour of T_c, the PG and T^* increase with decreasing doping in the UD region [1]. Two main scenarios dispute the origin of the pseudogap. In one of them the PG can be associated with preformed pairs that exist

above T_c. In the other one, the PG phase is distinct from superconductivity, and both compete [2, 3]. If the PG phase corresponds to a distinct order from superconductivity, another issue is whether T^* is a crossover or a true thermodynamical transition temperature [2, 3, 4]. Among the experimental probes angle-resolved photoemission spectroscopy [5, 6] (ARPES) and electronic Raman scattering [7] (ERS) have shown useful results for clarifying the nature of the nodal-antinodal dichotomy in the PG phase [2, 3]. Since these results are rather material-independent they can be assumed to be intrinsic features of the PG phase. Thus, it is desirable that ARPES and ERS are described by the same theory. In this paper we propose that the main features observed in ERS and ARPES can be analysed by self-energy effects in the proximity to the d-wave flux-phase instability [8, 9, 10]. This is the leading charge-ordered state that occurs in the framework of the t-J model in the large-N limit for the values of the electronic parameters suitable for cuprates [11]. Due to the fact that fluctuations of the flux-phase order parameter extend above its critical temperature, in the present scenario the PG can be viewed as a precursor effect. Thus, no phase transition occurs at T^*, and T^* is a crossover temperature.

ARPES shows below a characteristic temperature, called here T^{ARPES}, a PG at the antinodal momentum of the Fermi surface $\mathbf{k}_F^{AN}$ that vanishes around the nodal $\mathbf{k}_F^N$. Thus, instead of the expected large Fermi surface, disconnected Fermi arcs are observed for which the length increases with increasing doping and temperature [12, 13, 14, 15, 16, 17, 18]. Using specific configurations of the incident and scattered electric field with respect to the crystallographic axis, the B_{1g} and B_{2g} symmetry modes can be individually selected by ERS. While the B_{1g} mode probes electronic features around $\mathbf{k}_F^{AN}$, B_{2g} probes the vicinity of $\mathbf{k}_F^N$ (see insets in figure 4) [7]. Similarly to ARPES, ERS shows unconventional features in the normal state in the UD region. The most salient features are: (a) With decreasing temperature the slope of the B_{1g} response at $\omega = 0$ first increases, and below a characteristic temperature, called here T^{ERS}, decreases. This characteristic temperature follows the same trend as T^* [19, 20, 21]. Since the slope of the Raman spectra at $\omega = 0$ is proportional to the quasiparticle lifetime, the behaviour below T^{ERS} is clearly non-Fermi liquid, showing the non-Fermi liquid nature of the quasiparticles (QPs) near $\mathbf{k}_F^{AN}$. (b) The B_{2g} response shows a Fermi liquid behaviour, i.e., the slope increases with decreasing temperature showing the Fermi liquid nature of the QPs near $\mathbf{k}_F^N$ [19, 20, 21]. (c) The B_{2g} response shows a depletion at intermediate ω and relatively low doping [19, 22, 23, 24], and for which the origin and relation with the pseudogap has gained a renewed interest [25]. We show here that the features observed by these two experiments can be analysed, in the context of the t-J model, by self-energy effects in the proximity to the d-wave flux-phase instability.

The paper is organized as follows. In section 2 we present a summary of the theoretical framework. In section 3 we show the obtained results for ARPES and ERS and compare with the experiments. In section 4 we present the discussion and conclusion.

2. Summary of the theoretical framework

In the present study we use the t-J model

$$H = -\sum_{i,j,\sigma} t_{ij} \tilde{c}_{i\sigma}^\dagger \tilde{c}_{j\sigma} + J \sum_{\langle i,j \rangle} \left(\vec{S}_i \cdot \vec{S}_j - \frac{1}{4} n_i n_j \right) \tag{1}$$

where $t_{ij} = t \, (t')$ is the hopping between the first (second) nearest-neighbour sites on a square lattice, and J is the exchange interaction between the nearest-neighbour sites. $\langle i,j \rangle$ indicates a nearest-neighbour pair of sites. $\tilde{c}_{i\sigma}^\dagger$ ($\tilde{c}_{i\sigma}$) is the creation (annihilation) operator of electrons with spin σ ($\sigma = \downarrow, \uparrow$) in the Fock space without any double occupancy. $n_i = \sum_\sigma \tilde{c}_{i\sigma}^\dagger \tilde{c}_{i\sigma}$ is the electron density operator and $\vec{S}_i$ is the spin operator.

In the framework of the path integral large-N expansion [26, 27], the t-J model shows, in leading order, a paramagnetic Fermi liquid phase with electronic dispersion

$$\varepsilon_{\mathbf{k}} = -2 \left(t \frac{\delta}{2} + rJ \right) (\cos k_x + \cos k_y) - 4t' \frac{\delta}{2} \cos k_x \cos k_y - \mu, \tag{2}$$

where δ is the hole doping away from half-filling, and μ is the chemical potential. The chemical potential and r are calculated self-consistently [28, 29] from

$$r = \frac{1}{2N_s} \sum_{\mathbf{k}} \cos(k_x) n_F(\varepsilon_{\mathbf{k}}) \tag{3}$$

and

$$1 - \delta = \frac{2}{N_s} \sum_{\mathbf{k}} n_F(\varepsilon_{\mathbf{k}}) \tag{4}$$

where n_F is the Fermi function and N_s the number of sites. The parameter r contributes to the J-driven hopping term rJ, which is the second term between parenthesis in (2). This effective hopping term, which is not a bare electronic parameter, comes from the $J \sum_{\langle i,j \rangle} \vec{S}_i \cdot \vec{S}_j$ term of the t-J model. For more details about the path integral large-N expansion see [26, 27].

Hereafter, the appropriated parameters for cuprates $t'/t = -0.35$ and $J/t = 0.3$ are used. The hopping t and the lattice constant a of the square lattice are the energy and length units, respectively.

The paramagnetic Fermi liquid phase is unstable against a flux-phase [8, 9, 10, 11] below a transition temperature T_{FP} which decreases with increasing doping ending at a quantum critical point (QCP) [see solid line in figure 2(a)]. For $T < T_{FP}$, inside the flux-phase state, a true gap opens near $(\pi, 0)$ and the new Fermi surface consists of four small hole pockets near nodal direction. The flux-phase can be considered, in the framework of the microscopic t-J model, as a realization of the phenomenological proposed d-charge-density wave state [30]. It is worth highlighting that, with increasing T inside the flux-phase, the gap closes at T_{FP} [31]. In addition, a pair breaking-like peak is predicted in the B_{1g} mode in the normal state for $T < T_{FP}$ [31, 32]. However, ARPES shows that the PG fills with temperature [12, 17, 18], and ERS does not show clear signals of a peak in the normal state [19, 20, 21]. We will discuss herein that a crossover origin for the PG could describe these features.

In the paramagnetic Fermi liquid phase and in the proximity to the flux-phase instability, the carriers are mainly dressed, in next-to-leading order $[O(1/N)]$, by the self-energy $\Sigma(\mathbf{k}, \omega)$ (see [28, 29]), where

$$\text{Im}\,\Sigma(\mathbf{k}, \omega) = -\frac{1}{N_s} \sum_{\mathbf{q}} \gamma^2(\mathbf{q}, \mathbf{k}) \text{Im}\chi(\mathbf{q}, \omega - \varepsilon_{\mathbf{k-q}})$$
$$\times \left[n_F(-\varepsilon_{\mathbf{k-q}}) + n_B(\omega - \varepsilon_{\mathbf{k-q}}) \right], \tag{5}$$

In (5) n_B is the Bose factor, and

$$\chi(\mathbf{q}, \omega) = [8Jr^2 - \Pi(\mathbf{q}, \omega)]^{-1} \tag{6}$$

is the flux-phase susceptibility. $\chi(\mathbf{q}, \omega)$ diverges, at $\omega = 0$ and $\mathbf{Q} = (\pi, \pi)$, at T_{FP}. $\Pi(\mathbf{q}, \omega)$ is the electronic polarizability calculated with a form factor $\gamma(\mathbf{q}, \mathbf{k}) = 2rJ[\sin(k_x - q_x/2) - \sin(k_y - q_y/2)]$ [28, 29]. Note that since the instability is for $\mathbf{Q} = (\pi, \pi)$ the form factor $\gamma(\mathbf{q}, \mathbf{k})$ transforms into $\sim (\cos k_x - \cos k_y)$ which indicates the d-wave character of the flux-phase.

3. Comparison with ARPES and ERS experiments

3.1. ARPES

Using the Kramers-Kronig relation, $\text{Re}\Sigma(\mathbf{k}, \omega)$ can be determined from $\text{Im}\Sigma(\mathbf{k}, \omega)$, and the spectral function $A(\mathbf{k}, \omega)$ computed as usual

$$A(\mathbf{k}, \omega) = -\frac{1}{\pi} \frac{\text{Im}\Sigma(\mathbf{k}, \omega)}{[\omega - \epsilon_{\mathbf{k}} - \text{Re}\Sigma(\mathbf{k}, \omega)]^2 + [\text{Im}\Sigma(\mathbf{k}, \omega)]^2} \tag{7}$$

In figures 1(a) and 1(b) we show $A(\mathbf{k}, \omega)$ along the Fermi surface, i.e., from $\mathbf{k}_F^{AN}$ to $\mathbf{k}_F^N$, for the UD case $\delta = 0.11$ at $T = 0.025$ and $T = 0.07$, respectively. These calculations are in the paramagnetic Fermi liquid phase, where translational symmetry is not broken. While the spectral functions near $\mathbf{k}_F^N$ are sharp and develops a well pronounced QP peak, approaching $\mathbf{k}_F^{AN}$ the spectral functions become broad. At low temperature ($T = 0.025$) a PG is formed around $\mathbf{k}_F^{AN}$ [see arrow in figure 1(a)]. With increasing temperature ($T = 0.07$), the PG near $\mathbf{k}_F^{AN}$ fills, as seen in the experiment [13, 14]. Using the accepted value $t = 400$ meV for cuprates the leading edge of the PG is ~ 40 meV, which is of the order of the experimental value. In figure 1(c) we show $A(\mathbf{k}, \omega)$ for several temperatures at $\mathbf{k}_F^{AN}$ for the overdoped (OD) case $\delta = 0.28$. In contrast to UD, the spectral functions do not show any signal of a PG and, as expected for a Fermi liquid, the intensity at $\omega = 0$ decreases with increasing temperature. Figures 1(e)-(g) show an intensity plot for $A(\mathbf{k}, \omega = 0)$ for several dopings at $T = 0.02$. While for OD the full Fermi surface is observed, for UD we obtain Fermi arcs. Clearly, the length of Fermi arcs increases with increasing temperature and doping. It is worth mentioning that the behaviour of $\Sigma(\mathbf{k}, \omega)$ near $\omega = 0$ [figure 1(d)] is the cause of the PG formation and the non-Fermi liquid behaviour of QPs near $\mathbf{k}_F^{AN}$. While for overdoped $-\text{Im}\Sigma$ shows the expected minimum at $\omega = 0$ for both, $\mathbf{k}_F^N$ (not shown) and $\mathbf{k}_F^{AN}$, for underdoped $-\text{Im}\Sigma$ develops a pronounced maximum near $\mathbf{k}_F^{AN}$.
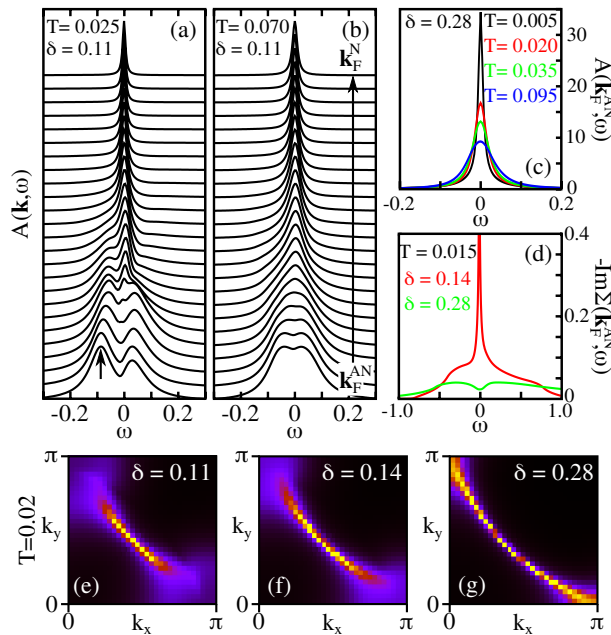
Figure 1. (a) and (b) Spectral functions from $\mathbf{k}_F^{AN}$ to $\mathbf{k}_F^N$ for doping $\delta = 0.11$, and for $T = 0.025$ and $T = 0.07$, respectively. (c) Spectral functions at $\mathbf{k}_F^{AN}$ for several temperatures for the overdoped case $\delta = 0.28$. (d) $-\mathrm{Im}\Sigma$ at $\mathbf{k}_F^{AN}$ as a function of ω for $T = 0.015$, and for $\delta = 0.14$ and $\delta = 0.28$. (e)-(g) Intensity plot for $A(\mathbf{k}, \omega = 0)$ at $T = 0.02$ for several dopings.

In figure 2(a), dashed line traces the temperature T^{ARPES}. For obtaining T^{ARPES} we calculate the loss of the low energy spectral weight $L = 1 - I_0/I$ at $\mathbf{k}_F^{AN}$, where I is the intensity of the spectral function at the leading edge of the PG [see arrow in figure 1(a)], and I_0 the intensity at $\omega = 0$ [13, 14]. In figure 2(b) we plot L versus T for $\delta = 0.11$, where L tends smoothly to zero indicating a crossover behaviour instead of a true phase transition. For the case of a true phase transition L should be exactly zero at the transition temperature. We use the criterion that T^{ARPES} is the temperature at which $L = 0.1$. In [13, 14] T^{ARPES} was obtained extrapolating $L \to 0$. In our case this criterion will give a slightly different T^{ARPES} [see doted line in figure 2 (b)]. Note that $T^{ARPES} \sim 200$ K for $\delta = 0.11$ is in a qualitative agreement with the experiments [13, 14]. Finally, although it is a crossover temperature and not the onset of an abrupt transition, T^{ARPES} terminates at the QCP.

For comparison with the ARPES signal, in figure 3 we show $A(\mathbf{k}, \omega)n_F(\omega)$ for $\mathbf{k_F} = (0.64, 0.25)\pi$ [panel (a)] and $\mathbf{k}_F^{AN}$ [panel (b)], for doping $\delta = 0.14$ and, for the two temperatures $T = 0.02 < T^{ARPES}$ and $T = 0.04 > T^{ARPES}$. See also the inset of panel (a) for the location of the two momenta on the Fermi surface. Note that $\mathbf{k_F} = (0.64, 0.25)\pi$ belongs to the arc region [figure 1(f)] for $T < T^{ARPES}$. For $\mathbf{k_F} = (0.64, 0.25)\pi$ we can see the expected behavior for a well defined QP, i.e., a well pronounced peak near $\omega = 0$ and the fast decay for $\omega > 0$ for both temperatures. The flat experimental background seen in the experiment was not included along with any additional broadening due, for instance, to impurities. The broadening of $A(\mathbf{k}, \omega)$ comes
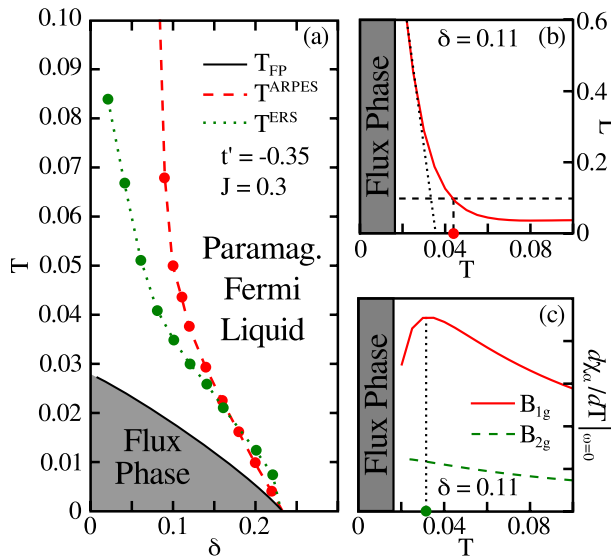
Figure 2. (a) Phase diagram in the T-δ plane. Dashed and dotted lines trace the crossover temperatures T^{ARPES} and T^{ERS}, respectively. In the grey region below solid line (T_{FP}) the flux-phase is frozen. (b) The loss of the low energy spectral weight L versus T for $\delta = 0.11$. The point at $T^{ARPES} = T \sim 0.04$ corresponds to the temperature where $L = 0.1$. Dotted line depicts the extrapolation of $L \to 0$. (c) Temperature dependence of the slope at $\omega = 0$ for both, the B_{1g} (solid line) and B_{2g} (dashed line) modes. The point at $T^{ERS} = T \sim 0.035$ corresponds to the temperature where the slope of the B_{1g} susceptibility at $\omega = 0$ starts to decrease with decreasing T.

only from $\Sigma(\mathbf{k}, \omega)$. While the changes with temperature are small for $\mathbf{k_F} = (0.64, 0.25)\pi$, they are stronger for $\mathbf{k}_F^{AN}$. As mentioned above, the temperature dependence of $\Sigma(\mathbf{k}, \omega)$ at the antinode is stronger than at the node, leading to the PG for $T < T^{ARPES}$ and broad spectral functions. The fact that the value for $A(\mathbf{k}_F^{AN}, \omega)n_F(\omega)$ at $\omega = 0$ is, in contrast to the expected behaviour for a Fermi liquid, smaller for $T = 0.02$ than for $T = 0.04$ indicates the PG formation at low temperatures.

In summary, this scenario leads to a PG and Fermi arcs which depend on doping and temperature, as seen in the experiments. The PG occurs due to the coupling between QPs and the flux-phase soft mode in the proximity to the instability. Other works have proposed that antiferromagnetic [33] and charge-density-wave [34] fluctuations in the proximity of the QCP may lead to a pseudogap. In present approach the PG phase is distinct from superconductivity and associated with short-ranged and short-lived fluctuations in the proximity to the flux-phase instability [28, 29]. Since this picture occurs in the paramagnetic phase for $T > T_{FP}$ there is no breaking of the translational symmetry, as suggested by the experiments [35]. Finally, it should be noted that the self-energy (5) is not phenomenological. This expression was derived beyond mean-field in a large-N framework of a path integral representation for the t-J model written in terms of Hubbard operators (see [28] and [29] and references therein). We suggest that the fact that our theory is supported by a controllable approach on the microscopic t-J
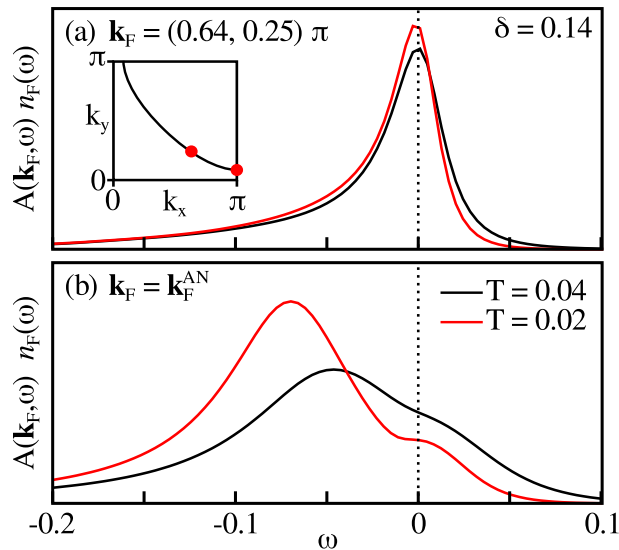
Figure 3. $A(\mathbf{k},\omega)n_F(\omega)$ for (a) $\mathbf{k_F} = (0.64, 0.25)\pi$ and (b) $\mathbf{k}_F^{AN}$, for doping $\delta = 0.14$ and, for the two temperatures $T = 0.02$ and $T = 0.04$. The inset in (a) shows the location of the two momenta on the Fermi surface.

model is an advantage over phenomenological proposals.

3.2. ERS

The electronic Raman response is calculated by the following susceptibility

$$\chi_\alpha(\omega) = \sum_{\mathbf{k}} \gamma_\alpha^2 \int d\varepsilon A(\mathbf{k}, \varepsilon) A(\mathbf{k}, \varepsilon - \omega)[n_F(\varepsilon - \omega) - n_F(\varepsilon)] \qquad (8)$$

where γ_α accounts for the Raman vertex in the geometry $\alpha = (B_{1g}, B_{2g})$ [7], i.e. $\gamma_{B_{1g}} = (t\delta/2 + rJ)(\cos k_x - \cos k_y)$ and $\gamma_{B_{2g}} = 4t'(\delta/2)\sin k_x \sin k_y$. In (8) we have neglected vertex corrections. A recent paper [36] shows that vertex corrections are small at low energy where the PG opens. In addition, the consistency of our results with the experiments (see below) shows that (8) captures important features.

Figures 4(a) and (b) show results for $\delta = 0.11$ for the B_{1g} and B_{2g} Raman modes, respectively. For B_{2g}, which probes the QPs near $\mathbf{k}_F^N$, the results are consistent with the expected ones from a Fermi liquid, i.e., the slope at $\omega = 0$ increases with decreasing T [see dashed line in figure 2(c)]. For B_{1g}, which probes QPs near $\mathbf{k}_F^{AN}$, the situation is quite different. The slope first increases with decreasing T, and below a temperature identified here as T^{ERS} this behaviour is reversed. The solid line in figure 2(c) shows the slope at $\omega = 0$ of the B_{1g} mode versus T for $\delta = 0.11$. In figure 2(a), dotted line traces T^{ERS} as a function of doping. Similar to T^{ARPES}, T^{ERS} is a crossover temperature that terminates at the QCP. In the OD side B_{1g} and B_{2g} show a Fermi liquid behaviour (not shown). It should be noted that high energy self-energy fluctuations, which may contribute to the flat spectrum at high frequency [19, 20, 21], are not considered. We focus on low energy features related to the pseudogap.
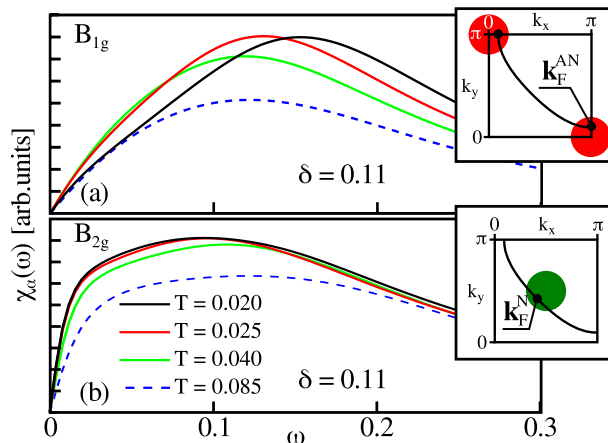
Figure 4. (a) and (b) B_{1g} and B_{2g} Raman response functions for $\delta = 0.11$, respectively, for several temperatures. The inset in (a) shows the location of $\mathbf{k}_F^{AN}$ and the region in the BZ selected by the B_{1g} mode. The inset in (b) shows the same as (a) but for $\mathbf{k}_F^{N}$ and the B_{2g} mode.

As mentioned in the introduction, ERS shows a depletion [19, 22, 23, 24] at intermediate energy for B_{2g} which has recently attracted a renewed interest [25]. In [25] the origin of this depletion was discussed in terms of a s-wave pseudogap. In the following we will propose an alternative explanation for the B_{2g} depletion. Figure 5(a) shows results for the B_{2g} mode for the low doping $\delta = 0.06$. Besides the increasing of the slope at $\omega = 0$ with decreasing T, a depletion at intermediate energy is obtained (see arrow) below $T \sim 0.05 \sim 230$ K. Since B_{2g} probes the nodal QPs, we identify this effect with the behaviour of $A(\mathbf{k}, \omega)$ near $\mathbf{k}_F^{N}$. In figure 5(b) we show results for the spectral function at $\mathbf{k}_F^{N}$ for $\delta = 0.06$ and several temperatures. The spectral functions show well defined QPs and, additionally, with decreasing T side-bands are developed (see arrows). These self-energy side-band effects, which reduce the QP weight at $\mathbf{k}_F^{N}$, are responsible for the depletion in B_{2g} at intermediate energy. Similar to the spectral function, $\Sigma(\mathbf{k}, \omega)$ at $\mathbf{k}_F^{N}$ [figures 4(c) and (d)] is Fermi liquid-like : $-\mathrm{Im}\Sigma(\mathbf{k}_F^{N}, \omega)$ shows always a minimum at $\omega = 0$ and some structure at $\omega \pm \sim 0.2$, and $\mathrm{Re}\Sigma(\mathbf{k}_F^{N}, \omega)$ shows a negative slope at $\omega = 0$. Thus, it is possible to extract the effective mass or dimensionless coupling parameter $\lambda = -\partial \mathrm{Re}\Sigma/\partial\omega|_{\omega=0}$. Since the Fermi liquid negative slope of $\mathrm{Re}\Sigma$ at $\omega = 0$ increases with decreasing temperature, λ increases with decreasing T. In figure 6(a) we show λ versus doping for several temperatures. Using the values for λ extracted for $\delta = 0.06$ the side-band features of figure 5(b) can be qualitatively reproduced [figure 6(b)].

Figure 6(a) shows that λ is strongly doping and temperature dependent, making the depletion at intermediate energy hardly visible for large doping. See for instance figure 4(b) for $\delta = 0.11$ where the depletion at intermediate energy is not visible. This doping dependence of λ is consistent with the fact that the depletion is not observed experimentally for large doping [19, 22, 23, 24]. Thus, the flux-mode which is very dominant at $\mathbf{q} \sim (\pi, \pi)$ and leads to the pseudogap near the antinode, possesses residual
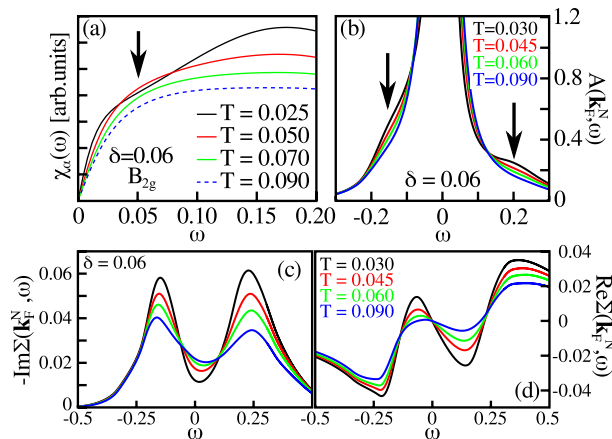
Figure 5. (a) B_{2g} response function for the low doping $\delta = 0.06$ and for several temperatures showing a depletion at intermediate energy (arrow). (b) Spectral functions for several temperatures at $\mathbf{k}_F^N$, for $\delta = 0.06$. Arrows show the side-band effects developed with decreasing temperature. (c) and (d) $-\text{Im}\Sigma$ and $\text{Re}\Sigma$, respectively, at $\mathbf{k}_F^N$ for $\delta = 0.06$ and several temperatures.

Fermi liquid-like interactions near the node. However, these residual interactions vanish with doping faster than the pseudogap. As in [25], our mechanism for the depletion has an origin on electronic correlation effects. It is linked to the PG in the sense that both, the depletion and the PG, come from the same self-energy. However, it would be precipitous to identify the B_{2g} depletion as the key to understanding the PG. For instance, the B_{2g} depletion disappears, in the experiment and in present theory, much faster with doping than the PG at $\mathbf{k}_F^{AN}$. We note that in [25] the B_{2g} depletion was studied only for doping $\delta = 0.05$. It will be interesting to discover whether the features obtained in [25] remain robust with increasing doping.

In spite of the qualitative agreement between present theory and the experiments on the B_{2g} depletion at intermediate energy, there are some unresolved issues arising from the phenomenology. Another possible origin for the depletion lies on the coupling between QPs and a bosonic mode [37]. In [37] a doping dependence of the bosonic coupling parameter λ was phenomenologically proposed in order to describe the experiments. It is worth mentioning that the proposed λ versus doping of [37] is close to the values obtained by ourselves [figure 6(a)]. In figure 6(c), using the band dispersion $\varepsilon_{\mathbf{k}}$ for $\delta = 0.11$, we show the B_{2g} depletion (see arrow) caused by a bosonic mode of characteristic frequency $\omega_D = 0.1$ and $\lambda = 0.4$. Since B_{2g} probes the nodal direction, the depletion could have the same origin as the nodal kink observed in ARPES [38, 39, 40]. Although it is controversial whether the origin of the kink is magnetic [41] or phononic [42, 43], it is fairly accepted that one possible origin is due to the coupling between QPs and a bosonic mode. Since the ARPES kink is observed from underdoped to overdoped [40], the question is why the bosonic mode associated with the kink is not seen in B_{2g} for the same doping range. On the other hand, if the bosonic mode is phononic in origin and isotropic in $\mathbf{k}$-space as expected from phonons [43], a similar depletion should also be
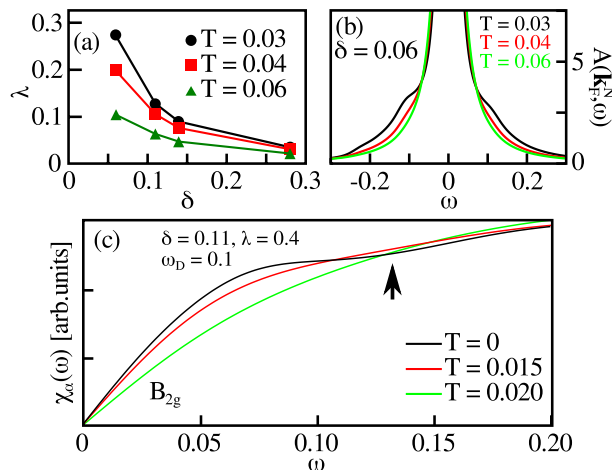
Figure 6. (a) The coupling $\lambda = -\partial \mathrm{Re}\Sigma/\partial\omega|_{\omega=0}$ as a function of δ for several temperatures. (b) Considering a bosonic mode with the couplings λ in (a) for $\delta = 0.06$ the side-band features of figure 5 (b) can be qualitatively reproduced. (c) B_{2g} response function for several temperatures obtained assuming a bosonic mode with $\lambda = 0.4$ and $\omega_D = 0.1$ for $\delta = 0.11$.

observed in B_{1g}, at least in overdoped where the low energy spectrum is not affected by the PG, and shows a Fermi liquid behaviour as B_{2g}. We conclude that more experiments and theory might be focused to discover why the excitations involved in the nodal kink are not clearly seen in ERS in the full range of doping.

4. Discussion and conclusion

In this paper we have discussed the PG as a precursor effect approaching the flux-phase instability. In this scenario T^* can be viewed as a crossover temperature and not as a true thermodynamical transition temperature, and the PG originates due to fluctuations which extend above the critical temperature T_{FP}. Thus, the PG occurs without the breaking of the translational symmetry. Nevertheless, it is important to bear in mind that present scenario requires that at sufficiently low temperature the flux-phase becomes thermodynamically stable below T_{FP}. Below T_{FP} the translational symmetry is broken and a Bragg reflection at (π, π) is expected, which is controversial from the experimental point of view. Thus, in order that our scenario be more reliable in comparison with experiments one should expect that the T_{FP} line exists at very low temperature and is sunk below the superconducting dome, being the normal state only affected by fluctuations. In addition, we should mention that below T_{FP} the Fermi surface transforms to closed Fermi pockets [28] for which observation is also controversial from ARPES. It should be noted that the reported Fermi pockets observed in quantum oscillations experiments at low temperature were discussed in the context of the d-charge-density-wave picture [44] which shows similar pockets to those expected from present theory below T_{FP}.

In conclusion, we have shown that self-energy effects in the proximity of a d-wave

flux-phase instability can account for the main features observed in ARPES and ERS experiments. It was shown that the doping and temperature dependence of the Fermi arcs and the pseudogap at the antinode correlate with the behaviour of the B_{1g} mode. In addition, the behaviour of the quasiparticles at the node correlates with the B_{2g} mode. We have also discussed the depletion at intermediate energy observed in the B_{2g} spectra.

Acknowledgments

References

[1] Timusk T and Statt B 1999 *Rep. Prog. Phys.* **62** 61
[2] Hüfner S, Hossain M A, Damascelli A and Sawatzky G A 2008 *Rep. Prog. Phys.* **71** 062501
[3] Norman M R, Pines D and Kallin C 2005 *Adv. Phys.* **54** 715
[4] Tallon J and Loram J 2001 *Physica C: Superconductivity* **349** 53 – 68
[5] Damascelli A, Hussain Z and Shen Z X 2003 *Rev. Mod. Phys.* **75** 473
[6] Lee W S, Vishik I M, Lu D H and Shen Z X 2009 *Journal of Physics: Condensed Matter* **21** 164217
[7] Devereaux T P and Hackl R 2007 *Rev. Mod. Phys.* **79**(1) 175–233
[8] Affleck I and Marston J B 1988 *Phys. Rev. B* **37**(7) 3774–3777
[9] Marston J B and Affleck I 1989 *Phys. Rev. B* **39**(16) 11538–11558
[10] Cappelluti E and Zeyher R 1999 *Phys. Rev. B* **59** 6475
[11] Bejas M, Greco A and Yamase H 2012 *Phys. Rev. B* **86** 224509
[12] Norman M R, Ding H, Randeris M, Campuzano J C, Yokoya T, Takeuchi T, Takahashi T, Mochiku T, Kadowaki K, Guptasarma P and Hinks D G 1998 *Nature (London)* **392** 157
[13] Kanigel A, Norman M R, Randeria M, Chatterjee U, Souma S, Kaminski A, Fretwell H M, Rosenkranz S, Shi M, Sato T, Takahashi T, Li Z Z, Raffy H, Kadowaki K, Hinks D, Ozyuzer L and Campuzano J C 2006 *Nat Phys* **2** 447–451
[14] Kanigel A, Chatterjee U, Randeria M, Norman M R, Souma S, Shi M, Li Z Z, Raffy H and Campuzano J C 2007 *Phys. Rev. Lett.* **99**(15) 157001
[15] Yoshida T, Hashimoto M, Ideta S, Fujimori A, Tanaka K, Mannella N, Hussain Z, Shen Z X, Kubota M, Ono K, Komiya S, Ando Y, Eisaki H and Uchida S 2009 *Phys. Rev. Lett.* **103**(3) 037004
[16] Kondo T, Khasanov R, Takeuchi T, Schmalian J and Kaminski A 2009 *Nature* **457** 296–300
[17] Hashimoto M, He R H, Tanaka K, Testaud J P, Meevasana W, Moore R G, Lu D, Yao H, Yoshida Y, Eisaki H, Devereaux T P, Hussain Z and Shen Z X 2010 *Nat. Phys.* **6** 414
[18] He R H, Hashimoto M, Karapetyan K, Koralek J D, Hinton J P, Testaud J P, Nathan V, Yoshida Y, Yao H, Tanaka K, Meevasana W, Moore R G, Lu D H, Mo S K, Ishikado M, Eisaki H, Hussain Z, Devereaux T P, Kivelson S A, Orenstein J, Kapitulnik A and Shen Z X 2011 *Science* **311** 1579
[19] Sacuto A, Benhabib S, Gallais Y, Blanc S, Cazayous M, Méasson M A, Wen J S, Xu Z J and Gu G D 2013 *Journal of Physics: Conference Series* **449** 012011
[20] Venturini F, Opel M, Devereaux T P, Freericks J K, Tüttő I, Revaz B, Walker E, Berger H, Forró L and Hackl R 2002 *Phys. Rev. Lett.* **89**(10) 107003
[21] Blumberg G, Kang M, Klein M V, Kadowaki K and Kendziora C 1997 *Science* **278** 1427–1432
[22] Nemetschek R, Opel M, Hoffmann C, Müller P F, Hackl R, Berger H, Forró L, Erb A and Walker E 1997 *Phys. Rev. Lett.* **78**(25) 4837–4840

[23] Opel M, Nemetschek R, Hoffmann C, Philipp R, Müller P F, Hackl R, Tüttő I, Erb A, Revaz B, Walker E, Berger H and Forró L 2000 *Phys. Rev. B* **61**(14) 9752–9774

[24] Gallais Y, Sacuto A, Devereaux T P and Colson D 2005 *Phys. Rev. B* **71**(1) 012506

[25] Sakai S, Blanc S, Civelli M, Gallais Y, Cazayous M, Méasson M A, Wen J S, Xu Z J, Gu G D, Sangiovanni G, Motome Y, Held K, Sacuto A, Georges A and Imada M 2013 *Phys. Rev. Lett.* **111**(10) 107001

[26] Foussats A and Greco A 2004 *Phys. Rev. B* **70**(20) 205123

[27] Foussats A, Greco A, Bejas M and Muramatsu A 2006 *Journal of Physics: Condensed Matter* **18** 11411

[28] Greco A 2009 *Phys. Rev. Lett.* **103**(21) 217001

[29] Greco A and Bejas M 2011 *Phys. Rev. B* **83**(21) 212503

[30] Chakravarty S, Laughlin R B, Morr D K and Nayak C 2001 *Phys. Rev. B* **63** 094503

[31] Zeyher R and Greco A 2002 *Phys. Rev. Lett.* **89**(17) 177004

[32] Zeyher R and Greco A 2004 *Physica C: Superconductivity* **408 - 410** 410 – 411

[33] Sedrakyan T A and Chubukov A V 2010 *Phys. Rev. B* **81**(17) 174536

[34] Perali A, Castellani C, Di Castro C and Grilli M 1996 *Phys. Rev. B* **54**(22) 16216–16225

[35] Norman M R, Kanigel A, Randeria M, Chatterjee U and Campuzano J C 2007 *Phys. Rev. B* **76** 174501

[36] Lin N, Gull E and Millis A J 2012 *Phys. Rev. Lett.* **109**(10) 106401

[37] Gallais Y, Tacon M L, Sacuto A and Colson D 2006 *EPL* **73** 594

[38] Zhou X J, Shi J, Yoshida T, Cuk T, Yang W L, Brouet V, Nakamura J, Mannella N, Komiya S, Ando Y, Zhou F, Ti W X, Xiong J W, Zhao Z X, Sasagawa T, Kakeshita T, Eisaki H, Uchida S, Fujimori A, Zhang Z, Plummer E W, Laughlin R B, Hussain Z and Shen Z X 2005 *Phys. Rev. Lett.* **95**(11) 117001

[39] Park S R, Cao Y, Wang Q, Fujita M, Yamada K, Mo S K, Dessau D S and Reznik D 2013 *Phys. Rev. B* **88**(22) 220503

[40] Park S R, Fukuda T, Hamann A, Lamago D, Pintschovius L, Fujita M, Yamada K and Reznik D 2014 *Phys. Rev. B* **89**(2) 020506

[41] Manske D, Eremin I and Bennemann K H 2001 *Phys. Rev. Lett.* **87**(17) 177005

[42] Lanzara A, Bogdanov P V, Zhou X J, Kellar S A, Feng D L, Lu E D, Yoshida T, Eisaki H, Fujimori A, Kishio K, Shimoyama J-I, Noda T, Uchida S, Hussain Z and Shen Z-X 2001 *Nature* **412** 510–514

[43] Zeyher R and Greco A 2001 *Phys. Rev. B* **64**(14) 140510

[44] Chakravarty S and Kee H Y 2008 *Proceedings of the National Academy of Sciences* **105** 8835–8839